Born−Oppenheimer Symmetry Breaking in the $\tilde{C}$ State of NO_2: Importance of Static and Dynamic Correlation Effects

Partha P. Bera, Yukio Yamaguchi, and Henry F. Schaefer, III*

Center for Computational Chemistry, University of Georgia, Athens, Georgia, 30602-2525

T. Daniel Crawford

Department of Chemistry, Virginia Tech, Blacksburg, Virginia, 24061

Received: September 19, 2007; In Final Form: December 10, 2007

A systematic theoretical treatment is performed with highly correlated ab initio theoretical methods to establish the structural nature of the $\tilde{C}$ state of NO_2. We predict the $\tilde{C}$ state to have an asymmetric structure (point group C_s). Spin-restricted and spin-unrestricted configuration interaction (CISD), coupled cluster [CCSD and CCSD(T)], multireference complete active space self-consistent field (CASSCF), and internally contracted multireference configuration interaction (ICMRCI) methods were used in conjunction with very large correlation-consistent polarized valence zeta cc-pVXZ and aug-cc-pVXZ [X = T, Q, 5] basis sets. The asymmetric $\tilde{C}\ ^2A''$ state is predicted to lie $T_e = 47.5$ kcal/mol (2.06 eV, 16600 cm^{-1}) above the $\tilde{X}\ ^2A_1$ state at the aug-cc-pV5Z/UCCSD(T) level of theory, with $T_0 = 46.0$ kcal/mol (2.00 eV, 16100 cm^{-1}), in good agreement with the experimental values of 46.77 kcal/mol (2.028 eV, 16360 cm^{-1}) by Weaver and 46.42 kcal/mol (2.013 eV, 16234 cm^{-1}) by Aoki. The symmetric structure (in C_{2v} symmetry) with $r_e(NO) = 1.274$ Å and θ_e (ONO) = 109.9° is a transition state between the two equivalent asymmetric (in C_s symmetry) structures and is located only 1.53 kcal/mol (0.066 eV, 540 cm^{-1}) above the asymmetric structure. The asymmetric structure is predicted to have structural parameters $r_e(NO_l) = 1.489$ Å, $r_e(NO_s) = 1.169$ Å, and $\theta_e(ONO) = 109.7°$ with the same method, aug-cc-pV5Z/UCCSD(T). The averaged NO bond distance is 1.329 Å, and the difference between the two NO bond distances is 0.320 Å. The three harmonic vibrational frequencies for the $\tilde{C}\ ^2A''$ state are 1656 (in-phase stretch), 759 (bend), and 378 (out- of-phase stretch) cm^{-1}. While these theoretical results further corroborate the previous predictions concerning the asymmetric nature of the $\tilde{C}$ state, there remains discrepancy between the theoretical and experimental symmetric stretching mode ω_1 (1656 and 923 cm^{-1}, respectively). It is possible, however, that this disagreement could be resolved by a reassignment of the corresponding lines in the experimental spectrum, though additional vibronic simulations of the spectrum are required to confirm this proposition.

I. Introduction

The environmentally active open-shell neutral molecule nitrogen dioxide (NO_2) poses significant resistance to the characterization of its electronic states.[1] Being a byproduct of industrialization and having vital import to environmental chemistry, NO_2 has found itself investigated many times from different directions. Several of its electronic states have been observed experimentally,[1−6] while others were predicted theoretically.[7−12] The low-lying doublet states are well-known to exhibit serious non-Born−Oppenheimer effects, including conical intersections between the $\tilde{X}\ ^2A_1$ and $\tilde{A}\ ^2B_2$ states and between the $\tilde{B}\ ^2B_1$ and $\tilde{C}\ ^2A_2$ states along the antisymmetric stretching vibrational mode, leading to a variety of very complex spectral features.[13−15] Furthermore, the $\tilde{X}-\tilde{B}$ states and $\tilde{A}-\tilde{C}$ states comprise two sets of Renner−Teller pairs, which are also subject to some relevant effects beyond the Born−Oppenheimer approximation. The $\tilde{C}$ state has been suggested[16,17] to have an asymmetric geometry. However, theory and experiment do not concur about the structure of the $\tilde{C}$ state.[18−20]

Gillespie and Khan, Wahl, Hosteny, and Krauss[8] used the multiconfiguration self-consistent field (MCSCF) method in 1975 to investigate electronic excited states of NO_2. One year later, the excited states of NO_2 were characterized theoretically in two pioneering paper by Jackels and Davidson.[9,10] This was followed in 1979 by the research of Handy, Goddard, and Schaefer.[11] These studies[8−11] predicted the $\tilde{C}\ ^2A_2$ state to have a ∼110° bond angle and a ∼1.27 Å NO distance in C_{2v} symmetry.

In 1989, Weaver, Metz, Bradforth, and Neumark[6] reported observation of the $\tilde{A}$ ($^2B_2$) and $\tilde{C}$ ($^2A_2$) states of NO_2 by negative ion photoelectron spectroscopy. In negative ion photoelectron spectroscopy, transitions occur directly from the anion ground electronic state to the ground and excited states of the neutral. Thus, the $\tilde{C}$ state is accessible via a one-electron photodetachment transition from NO_2^-, although the $\tilde{C}$ ($^2A_2$) ← $\tilde{X}$ ($^2A_1$) one-photon transition is electric dipole forbidden. Their experiment placed the excitation energy of the $\tilde{C}\ ^2A_2$ state from the ground $\tilde{X}\ ^2A_1$ state at $T_0 = 16360 \pm 70$ cm^{-1} (46.77 ± 0.20 kcal/mol, 2.028 ± 0.009 eV).

In 1991, Kaldor, while studying the symmetry-breaking properties of NO_2 and NO_3, predicted that the $\tilde{C}\ ^2A_2$ state may have a C_s instead of C_{2v} geometry.[16] At several correlated Fock

* To whom correspondence should be addressed. E-mail: hfs@uga.edu.

10.1021/jp077561y CCC: $40.75
Published on Web 03/01/2008

space based coupled cluster levels of theory, Kaldor reported the $\tilde{C}$ state to be symmetry broken with two unequal bond lengths, which contradicted the earlier predictions made by Jackels and Davidson.[9] At a DZP/CCSD level of theory, Kaldor predicted the C_s equilibrium geometry to be $r_e(NO_l) = 1.303$ for the long distance, $r_e(NO_s) = 1.274$ Å for the short distance, and $\theta_e(ONO) = 109.4°$. However, given the very small difference in energy between the C_{2v} and C_s geometries, Kaldor commented that "no concrete conclusion could be reached at this time regarding the symmetry of the $\tilde{C}$ state".

In the same year (1991), Burton, Yamaguchi, Alberts, and Schaefer studied excited-state Hartree−Fock analytic derivative anomalies for NO_2 and HCO_2 using the molecular orbital (MO) Hessian.[17] The MO Hessian is defined as the second derivatives of the electronic energy with respect to changes in the MO coefficients. For the $\tilde{C}\ ^2A_2$ state of NO_2, the SCF MO Hessian matrix presented three negative eigenvalues. The first root may be attributed to the symmetry-broken $^2A''$ wave function, while the second and third negative eigenvalues correspond to the low-lying $\tilde{X}\ ^2A_1$ and $\tilde{A}\ ^2B_2$ states. They have shown that the anomalous derivatives of some excited states are a direct result of the HF approximation, with the use of single configurations to describe the excited states. Employing the multireference complete active space SCF (CASSCF) method and the double-ζ plus polarization (DZP) basis set, they further investigated the molecular structures and energetics for the $^2A_2$ and $^2A''$ states of NO_2. For $^2A''$ NO_2, the near-full valence CASSCF [7a′, 3a″] and full valence CASSCF [9a′, 3a″] gave a C_s structure below the C_{2v} $^2A_2$ state, while smaller active space CASSCF [0a′, 3a″] and CASSCF [0a′, 5a″] presented a less-distorted C_s minimum. At the full valence DZP CASSCF [9a′, 3a″] level of theory, the $^2A''$ state structure was determined to be $r_e(NO_l) = 1.563$, $r_e(NO_s) = 1.185$ Å, and $\theta_e = 109.4°$.

The symmetry-forbidden dark $\tilde{C}\ ^2A_2$ state of NO_2 was explored by Shibuya, Kusumoto, Nagai, and Obi[19] in 1991 using optical−optical double resonance (OODR) spectroscopy. From the first rotationally resolved OODR spectrum, they extracted the approximate geometric parameters $r \sim 1.4$ Å and $\theta \sim 102°$, which disagreed with the theoretical results of both Gillespie[8] and Jackels and Davidson.[9]

In the wake of this discrepancy between the theory and the experiment, Crawford and Schaefer[18] investigated the rotational constants of the $\tilde{C}\ ^2A_2$ state using high-level ab initio quantum mechanical methods with large basis sets. Crawford's 1993 systematic work agreed with the previous theoretical results and contradicted the experimental geometry inferred by Shibuya et al.[19] Crawford predicted the $\tilde{C}$ state to have a 1.280 Å NO bond distance and a 109.8° ONO bond angle at the TZ2P+f/CCSD-(T) level of theory.[18]

In 1996, Aoki, Hoshina, and Shibuya[21] reported the fluorescence spectrum of NO_2. Aoki et al. assigned the $\tilde{C}\ ^2A_2$ state to $T_0 = 16220 \pm 20$ cm^{-1}, estimated from dispersed fluorescence spectra, and $T_0 = 16234$ cm^{-1} from OODR analysis with respect to the $\tilde{X}\ ^2A_1$ ground state. They deduced the $^2A_2$ state of NO_2 to have a 1.339 Å bond length and a 108.4° ONO bond angle and refined the results reported by the same group 5 years before. On the basis of the assumption that the $\tilde{C}$ state has C_{2v} symmetry, they assigned the vibrational spectrum; $\omega_1(a_1) = 1010$, $\omega_2(a_1) = 750$, and $\omega_3(b_2) = 250$ cm^{-1}. Their new experimental geometrical parameters provided much better accord with the theoretical predictions than the earlier experimental values by the same group,[19] who had reported a 102° bond angle. However, they did not report any evidence of a C_s geometry for the $\tilde{C}$ state, as predicted by Kaldor[16] and by Burton.[17]

Another experimental method to approach the dark (from the ground state) $\tilde{C}$ state is the observation of the $\tilde{D}-\tilde{C}$ fluorescence after the excitation of NO_2 to the highly excited $\tilde{D}\ ^2B_2$ state. Shibuya and co-workers[22] analyzed the vibrational level structures of $\tilde{C}\ ^2A_2$ in the excitation energy region of 16 200−21 000 cm^{-1} on the basis of NO_2 $\tilde{D}\ ^2B_2$ (0,0,0)−$\tilde{C}\ ^2A_2$ (n_1, n_2, n_3) fluorescence spectra measured with a multichannel photodetection system. About 36 vibrational levels were identified from the observed spectra of each of two isotopically labeled $^{14}NO_2$ and $^{15}NO_2$. Although the excitation energy measured in the latter, 16234 cm^{-1} (46.42 kcal/mol, 2.013 eV), was essentially the same as that reported by Aoki, the vibrational assignment of the spectra led to different conclusions from those presented earlier.[21] Assuming the $\tilde{C}$ state has C_{2v} symmetry, it was not possible to assign all of the peaks on the vibrational progression. However, if the molecule had two unequal bond distances—and hence C_s symmetry—the vibrational progression could be assigned completely (see Figure 3 of Shibuya et al.[22]). Isotopic substitution of nitrogen with ^{15}N seems to have corroborated the argument. The three harmonic vibrational frequencies reported by Shibuya were $\omega_1 = 923$, $\omega_2 = 756$, and $\omega_3 = 273$ cm^{-1}.

In 1997, Crawford, Stanton, Szalay, and Schaefer,[20] in a detailed theoretical study, predicted that the $\tilde{C}$ state may have a C_s equilibrium geometry. Using DZP and cc-pVTZ basis sets and various coupled cluster with singles, doubles, and triples [CCSD, CCSD(T) and CCSDT] methods, they predicted that the $\tilde{C}\ ^2A_2$ state (in C_{2v} point group symmetry) has an imaginary antisymmetric stretching vibrational frequency for unrestricted (UHF) and quasi-restricted Hartree−Fock (QRHF) references. For spin-restricted open-shell (ROHF) Hartree−Fock references, however, the corresponding imaginary frequency did not appear until the coupled cluster wave function was improved to include full triple excitations (CCSDT). This phenomenon was attributed to a b_2 symmetry instability in the ROHF orbital Hessian, which did not appear in the UHF or QRHF Hessians. Furthermore, Crawford et al. speculated that the source of the symmetry breaking observed in the UHF- and QRHF-based CCSD, CCSD-(T), and CCSDT calculations as well as at the ROHF-CCSDT level could arise from a pseudo-Jahn−Teller interaction between the $\tilde{C}\ ^2A_2$ state and the $\tilde{B}\ ^2B_1$ state, which lies higher in energy at the optimized C_{2v} geometry of the $\tilde{C}$ state. At the DZP UHF-CCSD(T) level of theory, they found a C_s structure of $r_e(NO_l) = 1.513$, $r_e(NO_s) = 1.183$ Å, and $\theta_e = 109.5°$. Crawford et al.[20,23] stated that the $\tilde{C}$ state may have C_s symmetry, and due to the small barrier in the double well antisymmetric stretching potential, the dynamical symmetry seen by the experiments was C_{2v}. However, the work lacked a description of the vibrational frequencies associated with the C_s equilibrium geometry.

In 2005, Wiberg et al.[24] predicted a 1.27 Å bond length and a 109° bond angle for the $\tilde{C}\ ^2A_2$ state at the CIS and EOM-CCSD levels of theory with a 6-311++G** basis set. However, they did not explore the possibility of the $\tilde{C}$ state having C_s geometry.

In the present research, we have approached the $\tilde{C}\ ^2A_2$ and the $\tilde{C}\ ^2A''$ stationary points from the following points of view. In lieu of the discrepancy between theoretical and experimental equilibrium geometries, we have investigated the $\tilde{C}$ state using highly correlated ab initio coupled cluster methods. A systematic study of the ground $\tilde{X}\ ^2A_1$ and the $\tilde{C}\ ^2A_2$ and $\tilde{C}\ ^2A''$ structures was also carried out at the multireference CASSCF and ICMRCI

TABLE 1: Three Dominant Configurations of the cc-pVTZ/MRCI Wave Function for the $\tilde{C}\ ^2A_2$ and $\tilde{C}\ ^2A''$ States of NO_2[a]

$^2A_2$		$^2A''$	
configuration	coefficient	configuration	coefficient
$...(6a_1)^2(1b_1)^2(2b_1)^0(4b_2)^2(1a_2)$	$C_1 = 0.897$	$...(9a')^2(10a')^2(11a')^0(1a'')^2(2a'')(3a'')^0$	$C_1 = 0.908$
$...(6a_1)^2(1b_1)(2b_1)(4b_2)^2(1a_2)$	$C_2 = -0.213$	$...(9a')^2(10a')^2(11a')^0(1a'')^0(2a'')(3a'')^2$	$C_2 = -0.139$
$...(6a_1)^2(1b_1)^0(2b_1)^2(4b_2)^2(1a_2)$	$C_3 = -0.124$	$...(9a')^2(10a')^0(11a')^2(1a'')^2(2a'')(3a'')^0$	$C_3 = -0.134$

[a] Note: The $\tilde{C}\ ^2A_2$ state is at C_{2v} [$r_e(NO) = 1.2805$ Å and $\theta_e = 109.86°$] geometry. The $\tilde{C}\ ^2A''$ state is at C_s [$r_e(NO_l) = 1.5042$ Å, $r_e(NO_s) = 1.1723$ Å, and $\theta_e = 109.63°$] geometry.

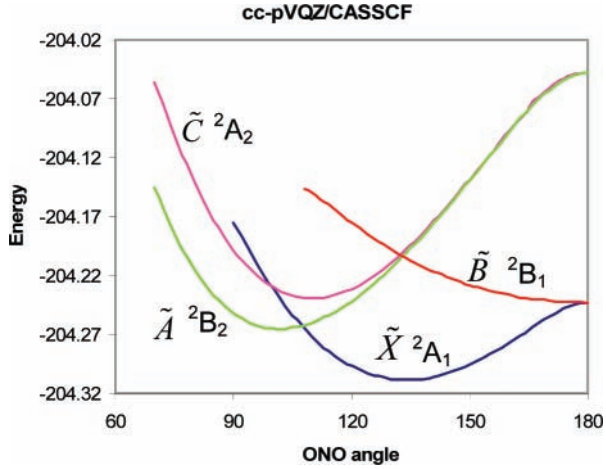

Figure 1. Potential energy diagram for the four lowest-lying doublet electronic states of NO_2 in C_{2v} symmetry, predicted at the cc-pVQZ/CASSCF level of theory; the energy is in hartree, and angles are in degrees.

levels of theory. The significance of static (nondynamical) and dynamical correlation effects in characterizing the excited electronic $\tilde{C}$ state of NO_2 is addressed.

II. Electronic Structure Considerations

The $\tilde{X}\ ^2A_1$ ground electronic state of NO_2 has the following electronic configuration

$$[\text{core}](3a_1)^2(2b_2)^2(4a_1)^2(3b_2)^2(1b_1)^2(5a_1)^2(1a_2)^2(4b_2)^2(6a_1) \quad \tilde{X}^2A_1,$$

where [core] denotes the three lowest-lying core [N,O: 1s like] orbitals, namely $1a_1$, $1b_2$, and $2a_1$.

The $\tilde{A}\ ^2B_2$ state arises from an excitation $6a_1 \leftarrow 4b_2$

$$[\text{core}](3a_1)^2(2b_2)^2(4a_1)^2(3b_2)^2(1b_1)^2(5a_1)^2(1a_2)^2(4b_2)(6a_1)^2 \quad \tilde{A}\ ^2B_2.$$

A single excitation from $6a_1$ to $2b_1$ gives the $\tilde{B}\ ^2B_1$ state

$$[\text{core}](3a_1)^2(2b_2)^2(4a_1)^2(3b_2)^2(1b_1)^2(5a_1)^2(1a_2)^2(4b_2)^2(2b_1) \quad \tilde{B}\ ^2B_1.$$

The $\tilde{C}\ ^2A_2$ state originates from the ground $\tilde{X}\ ^2A_1$ state via a $6a_1 \leftarrow 1a_2$ single excitation

$$[\text{core}](3a_1)^2(2b_2)^2(4a_1)^2(3b_2)^2(1b_1)^2(5a_1)^2(1a_2)(4b_2)^2(6a_1)^2 \quad \tilde{C}\ ^2A_2.$$

The $\tilde{C}\ ^2A''$ state has the following electronic configuration

$$[\text{core}](4a')^2(5a')^2(6a')^2(7a')^2(1a'')^2(8a')^2(9a')^2(10a')^2(2a'') \quad \tilde{C}\ ^2A''.$$

TABLE 2: Theoretical Predictions of the Total Energy (in Hartree), Dipole Moment (in Debye), and Harmonic Vibrational Frequencies (in cm^{-1}) for the $\tilde{C}\ ^2A_2$ Electronic State of NO_2

level of theory	energy	μ_e	$\omega_1(a_1)$	$\omega_2(a_1)$	$\omega_3(b_2)$
cc-pVQZ/ROHF	−204.054923	0.061	1623	899	2897
aug-cc-pVQZ/ROHF	−204.056277	0.061	1621	898	2892
cc-pV5Z/ROHF	−204.058960	0.063	1622	899	2893
aug-cc-pV5Z/ROHF	−204.059338	0.062	1621	899	2892
cc-pVQZ/RCISD	−204.669237	0.047	1502	843	3139
aug-cc-pVQZ/RCISD	−204.674724	0.056	1500	843	3133
cc-pV5Z/RCISD	−204.687159	0.054	1505	845	3156
aug-cc-pV5Z/RCISD	−204.689452	0.057	1504	845	3155
cc-pVQZ/UCISD	−204.669955	0.046	1501	843	3145
aug-cc-pVQZ/UCISD	−204.675444	0.055	1499	843	3139
cc-pV5Z/UCISD	−204.687873	0.053	1504	845	3163
aug-cc-pV5Z/UCISD	−204.690166	0.056	1503	845	3162
cc-pVQZ/RCCSD	−204.747188	0.043	1397	802	1589
aug-cc-pVQZ/RCCSD	−204.753617	0.057	1395	801	1587
cc-pV5Z/RCCSD	−204.766653	0.053	1400	804	1605
aug-cc-pV5Z/RCCSD	−204.769267	0.057	1398	803	1605
cc-pVQZ/UCCSD	−204.749640	0.041	1384	798	720
aug-cc-pVQZ/UCCSD	−204.756081	0.055	1381	797	719
cc-pV5Z/UCCSD	−204.769130	0.051	1386	800	732
aug-cc-pV5Z/UCCSD	−204.771748	0.055	1385	799	732
cc-pVQZ/RCCSD(T)	−204.783327	0.048	1320	771	1251
aug-cc-pVQZ/RCCSD(T)	−204.790518	0.067	1316	770	1247
cc-pV5Z/RCCSD(T)	−204.804070	0.061	1321	773	1262
aug-cc-pV5Z/RCCSD(T)	−204. 806986	0.067	1320	772	1262
cc-pVQZ/UCCSD(T)	−204.784521	0.048	1317	770	378
aug-cc-pVQZ/UCCSD(T)	−204.791716	0.067	1314	770	363
cc-pV5Z/UCCSD(T)	−204.805272	0.061	1319	772	377
aug-cc-pV5Z/UCCSD(T)	−204.808189	0.067	1317	772	372
cc-pVQZ/CASSCF	−204.239390	0.024	1288	766	749i
aug-cc-pVQZ/CASSCF	−204.240639	0.027	1288	766	749i
cc-pV5Z/CASSCF	−204.243354	0.028	1289	766	749i
aug-cc-pV5Z/CASSCF	−204.243699	0.027	1288	766	749i
cc-pVTZ/ICMRCI	−204.677024	0.034	1299	764	573i
aug-cc-pVTZ/ICMRCI	−204.690718	0.059	1294	763	579i
cc-pVQZ/ICMRCI	−204.731450	0.043	1314	771	555i
aug-cc-pVQZ/ICMRCI	−204.737096	0.054	1312	771	556i
DZP/UHF-CCSD(T)[a]	−204.589748		1309	756	563i
cc-pVTZ/UHF-CCSD(T)[a]	−204.759768		1328	773	583i
cc-pVQZ/UHF-CCSD(T)[a]	−204.873605		1335	778	579i
experiment, ref 18			1010	740	250
experiment, ref 19			1065	772	

[a] Vibrational frequencies taken from the 1997 paper of Crawford et al. (ref 20).

The three largest CI coefficients of the cc-pVTZ/ICMRCI wave functions for the $\tilde{C}\ ^2A_2$ C_{2v} [$r_e(NO) = 1.2805$ Å and $\theta_e = 109.86°$] and $\tilde{C}\ ^2A''$ [$r_e(NO_l) = 1.5042$ Å, $r_e(NO_s) = 1.1723$ Å, and $\theta_e = 109.63°$] states are associated with the electron configurations presented in Table 1. Two major contributions to the MRCI wave function come from the $1b_1 \rightarrow 2b_1$ and $1b_1^2 \rightarrow 2b_1^2$ excitations for the $\tilde{C}\ ^2A_2$ and from double excitations of the $1a''^2 \rightarrow 3a''^2$ and $10a'^2 \rightarrow 11a'^2$ types for the $\tilde{C}\ ^2A''$ state.

TABLE 3: Theoretical Predictions of the Total Energy (in Hartree), Dipole Moment (in Debye), Harmonic Vibrational Frequencies (in cm^{-1}), and Zero-Point Vibrational Energy (ZPVE in kcal/mol) for the $\tilde{C}\ ^2A''$ Electronic State of NO_2

level of theory	energy	μ_e	$\omega_1(a')$	$\omega_2(a')$	$\omega_3(a')$	ZPVE
cc-pVQZ/ROHF	−204.083562	0.397	2001	984	729	5.31
aug-cc-pVQZ/ROHF	−204.084965	0.405	2000	983	730	5.31
cc-pV5Z/ROHF	−204.087640	0.403	2000	984	730	5.31
aug-cc-pV5Z/ROHF	−204.088034	0.405	2000	984	730	5.31
cc-pVQZ/RCISD	−204.680824	0.501	1855	883	623	4.80
aug-cc-pVQZ/RCISD	−204.686344	0.519	1855	881	623	4.80
cc-pV5Z/RCISD	−204.698737	0.506	1858	885	627	4.82
aug-cc-pV5Z/RCISD	−204.701036	0.512	1857	884	627	4.81
cc-pVQZ/UCISD	−204.681010	0.498	1854	883	623	4.80
aug-cc-pVQZ/UCISD	−204.686533	0.516	1854	881	622	4.80
cc-pV5Z/UCISD	−204.698924	0.504	1857	885	626	4.81
aug-cc-pV5Z/UCISD	−204.701224	0.509	1856	884	626	4.81
cc-pVQZ/RCCSD	−204.753601	0.565	1726	814	516	4.37
aug-cc-pVQZ/RCCSD	−204.760075	0.595	1726	811	513	4.36
cc-pV5Z/RCCSD	−204.773022	0.575	1728	815	518	4.38
aug-cc-pV5Z/RCCSD	−204.775644	0.583	1728	814	518	4.37
cc-pVQZ/UCCSD	−204.754294	0.519	1700	810	492	4.29
aug-cc-pVQZ/UCCSD	−204.760780	0.548	1700	807	489	4.28
cc-pV5Z/UCCSD	−204.773732	0.527	1700	811	494	4.30
aug-cc-pV5Z/UCCSD	−204.776359	0.536	1700	810	493	4.29
cc-pVQZ/RCCSD(T)	−204.786491	0.741	1674	760	405	4.06
aug-cc-pVQZ/RCCSD(T)	−204.793743	0.792	1676	757	400	4.05
cc-pV5Z/RCCSD(T)	−204.807157	0.758	1675	762	404	4.06
aug-cc-pV5Z/RCCSD(T)	−204.810084	0.772	1675	760	403	4.06
cc-pVQZ/UCCSD(T)	−204.787024	0.701	1656	760	381	4.00
aug-cc-pVQZ/UCCSD(T)	−204.794286	0.752	1658	756	376	3.99
cc-pV5Z/UCCSD(T)	−204.807702	0.715	1655	761	380	4.00
aug-cc-pV5Z/UCCSD(T)	−204.810634	0.729	1656	759	378	3.99
cc-pVQZ/CASSCF	−204.245058	1.101	1720	713	339	3.96
aug-cc-pVQZ/CASSCF	−204.246267	1.109	1719	715	341	3.97
cc-pV5Z/CASSCF	−204.248990	1.109	1719	714	340	3.96
aug-cc-pV5Z/CASSCF	−204.249314	1.108	1719	715	341	3.97
cc-pVTZ/ICMRCI	−204.679668	0.742	1649	748	356	3.94
aug-cc-pVTZ/ICMRCI	−204.693474	0.802	1649	744	356	3.93
cc-pVQZ/ICMRCI	−204.733694	0.686	1642	761	357	3.95
aug-cc-pVQZ/ICMRCI	−204.739348	0.708	1641	760	357	3.94
experiment, ref 22			923	756	273	

III. Theoretical Methods

Hartree−Fock and post-Hartree−Fock ab initio electronic structure methods were used to determine the total energies, geometries, and physical properties of NO_2 at its $\tilde{C}\ ^2A_2$ and $\tilde{C}\ ^2A''$ stationary points. Dunning's correlation-consistent polarized valence basis sets cc-pVXZ[25] and augmented cc-pVXZ (where X = T, Q, and 5)[26] were used to systematically study basis set expansion effects. Self-consistent field (SCF), configuration interaction singles and doubles (CISD), coupled cluster singles and doubles (CCSD),[27−29] and CCSD with perturbative triples [CCSD(T)][29−31] corrections were employed to improve upon the starting restricted open-shell Hartree−Fock (ROHF) wave functions in a single-reference framework. The full valence complete active space self-consistent field (CASSCF) method included 17 electrons in 12 orbitals (2s and 2p of N and O). Internally contracted multireference configuration interaction (ICMRCI)[32] methods were also used to investigate static (nondynamical) correlation effects. The computations were performed using the MOLPRO ab initio quantum chemistry package.[33] At the correlated levels of theory, the harmonic vibrational frequencies were determined by numerical differentiation of total energies of the electronic states at their respective equilibrium geometries. Some harmonic vibrational frequencies were also computed using ACESII[34] and PSI3[35] quantum chemistry packages. The dipole moments were evaluated from the finite differences of total energies obtained by applying a small electric field as a perturbation at the equilibrium geometries. Zero-point vibrational energies (ZPVEs) were computed from the harmonic vibrational frequencies.

IV. Results and Discussion

A systematic study of the description of correlation and basis set effects for the total energies and harmonic vibrational frequencies of the $\tilde{C}\ ^2A_2$ and $\tilde{C}\ ^2A''$ stationary points was performed using single-reference ROHF, RCISD, UCISD, RCCSD, UCCSD, RCCSD(T), and UCCSD(T) as well as the multireference CASSCF and ICMRCI methods. The analogous total energies and physical properties of the $\tilde{X}\ ^2A_1$ ground state[36] were used for comparison with the excited-state properties. Potential energy curves with respect to the valence angle, in C_{2v} symmetry, for the four lowest-lying doublet states at the cc-pVQZ/CASCF level of theory are depicted in Figure 1. The NO bond distance is optimized at a fixed bond angle to minimize the total energy. It is evident from Figure 1 that the bond angles for the $\tilde{A}\ ^2B_2$ and $\tilde{C}\ ^2A_2$ states are smaller than that for the $\tilde{X}\ ^2A_1$ state at their respective equilibrium geometries. The $\tilde{X}\ ^2A_1$ and $\tilde{B}\ ^2B_1$ states connect to the doubly degenerate $^2\Pi_u$ state at linearity, while the $\tilde{A}\ ^2B_2$ and $\tilde{C}\ ^2A_2$ states coalesce to the $^2\Pi_g$ state for linear configurations. Therefore, the $\tilde{X}-\tilde{B}$ states and $\tilde{A}-\tilde{C}$ states comprise two sets

TABLE 4: Theoretical Predictions of the Harmonic Vibrational Frequencies (in cm^{-1}) for the C̃ $^2A''$ State of $^{14}NO_2$ and $^{15}NO_2$ Molecules Using the CCSD, CCSD(T), and ICMRCI Methods

	$^{14}NO_2$			$^{15}NO_2$			Isotopic Shifts		
level of theory	$\omega_1(\sigma^+)$	$\omega_2(\pi)$	$\omega_3(\sigma^+)$	$\omega_1(\sigma^+)$	$\omega_2(\pi)$	$\omega_3(\sigma^+)$	$\Delta(\omega_1)$	$\Delta(\omega_2)$	$\Delta(\omega_3)$
cc-pVQZ/UCCSD	1727	814	516	1697	784	498	29	15	4
aug-cc-pVQZ/UCCSD	1726	811	514	1697	796	509	29	15	4
cc-pV5Z/UCCSD	1728	815	518	1698	800	513	30	15	4
aug-cc-pV5Z/UCCSD	1728	814	518	1698	799	513	30	15	5
cc-pVQZ/CCSD(T)	1674	761	405	1645	747	401	29	13	4
aug-cc-pVQZ/CCSD(T)	1675	757	398	1647	744	396	29	14	4
cc-pV5Z/CCSD(T)	1675	761	404	1646	749	400	29	13	4
aug-cc-pV5Z/CCSD(T)	1675	760	403	1646	747	399	29	13	4
cc-pVTZ/ICMRCI	1649	748	356	1621	736	352	28	13	4
aug-cc-pVTZ/ICMRCI	1649	744	356	1621	732	353	28	12	3
cc-pVQZ/ICMRCI	1642	761	357	1614	748	353	29	13	4
aug-cc-pVQZ/ICMRCI	1641	760	357	1613	748	353	28	13	4
Expt. (ref 22) assignment									Expt. $\Delta(\omega)$
(0,0,1)			256			257			1
(0,0,2)			600			600			0
(0,1,0)/(0,0,3)		747			738				9
(1,0,0)	970			945					25
(0,1,1)/(0,0,4)	1010			999					11
(0,1,2)	1310			1293					17
(0,2,0)/(0,1,3)	1481			1469					12
(1,1,0)	1690			1658					32
(0,2,1)/(0,1,4)	1746			1731					15
(0,2,2)	2021			1999					22
(0,1,5)	2095			2072					23

of Renner−Teller pairs. The crossing of the C̃ and B̃ states seen in Figure 1 will turn into a conical intersection by activating the asymmetric stretching vibration of NO_2. This conical intersection is of similar origin as that between X̃ and Ã states.

The predicted total energies, dipole moments, and harmonic vibrational frequencies for the C̃ $^2A_2$ state are presented in Table 2 with single and multireference levels of theory. The dipole moment of the X̃ $^2A_1$ state is determined to be 0.33 Debye at the aug-cc-pV5Z/UCCSD(T) level of theory, with the dipole pointing toward the oxygen atoms ($^+NO_2^-$).[36] For the symmetric C̃ $^2A_2$ state, the dipole moment is predicted to be 0.07 Debye ($^+NO_2^-$) with the same method. The magnitude of the dipole moment is significantly smaller for the C̃ $^2A_2$ state compared to that of the X̃ $^2A_1$ state. The symmetric (a_1) harmonic vibrational modes (ω_1, ω_2) of the C̃ $^2A_2$ state show nice convergence with respect to treatment of correlation effects and basis set size. However, the harmonic frequencies for the antisymmetric (b_2) stretching mode show a range of peculiar and unphysical frequencies with both the restricted and unrestricted wave functions. The unphysical b_2 symmetry vibrational frequencies have been confirmed with multiple quantum chemistry packages. The RCCSD and RCCSD(T) methods give significantly different b_2 frequencies than their unrestricted counterparts UCCSD and UCCSD(T), although their geometries do not differ by much. It should be noted that both the RCC and UCC models provided by the MOLPRO package make use of ROHF reference determinants. Hence, the finding that the harmonic frequency associated with the b_2 mode is real is consistent with the earlier wok of Crawford et al.,[20] who found that, for ROHF reference functions, at least the full singles, doubles, and triples (CCSDT) model is necessary to obtain an imaginary b_2 vibrational frequency. UHF and QRHF references, on the other hand, yield the apparently correct imaginary frequency starting at the CCSD level of theory.

As noted earlier by Crawford et al.,[20] the disagreement between the UHF- and ROHF-based CC results above arises in part from an instability in the ROHF MO Hessian that does not appear in the corresponding UHF MO Hession. However, the occasional presence of such instabilities warrants caution as to the reliability of single-reference methods when describing states exhibiting potential pseudo-Jahn−Teller interactions.[37] Therefore, the CASSCF and CASSCF-MRCI multireference methods were used to investigate the static (nondynamical) correlation effects for the vibrational frequencies. Both of these levels of theory with all of the basis sets predict the C̃ $^2A_2$ state to have imaginary antisymmetric stretching vibrational frequencies, as presented in Table 2. At the aug-cc-pVQZ/ICMRCI level, the C̃ $^2A_2$ state has an antisymmetric imaginary frequency of 556i cm^{-1}. Consequently, the C̃ electronic state of NO_2 prefers a C_s structure rather than C_{2v}, at least at the CASSCF and ICMRCI levels of theory. It is observed that the static (nondynamic) correlation effects are important to correctly reproduce the shape of the potential energy surface at the C_{2v} stationary point. In this light, the significance of including the higher excitations (at least single, double, and full triple excitations) for the single-reference wave functions should also be realized.[20]

The total energies, dipole moments, and harmonic vibrational frequencies of the C̃ $^2A''$ state are reported in Table 3. The dipole moment of the asymmetric C̃ $^2A''$ state is predicted to be considerably larger in magnitude than that for the C̃ $^2A_2$ stationary point and increases with advanced treatments of correlation effects, simultaneous with the increasing asymmetric nature of the two NO bonds. At the aug-cc-pV5Z/UCCSD(T) level of theory, the dipole moment is predicted to be 0.73 Debye. The harmonic vibrational frequencies are 1656 cm^{-1} for symmetric stretching (ω_1) and 759 cm^{-1} for bending (ω_2) with the same method. The relatively high symmetric stretching frequency is the reflection of the very short NO bond. At this C_s symmetry equilibrium geometry, the antisymmetric stretching frequency (ω_3) is real and consistent with the change in the

TABLE 5: Optimized Structures of the $\tilde{C}\ ^2A_2$ and $\tilde{C}\ ^2A''$ Stationary Points of NO_2. The Bond Distances are in Å, and the Angles are in Degrees. The Abbreviation (av) Indicates the Average of the Two Bond Lengths, and Δr Denotes Their Difference

	$\tilde{C}\ ^2A_2$		$\tilde{C}\ ^2A''$				
level of theory	r_e(NO)	θ_e(ONO)	$r_e(NO_l)$	$r_e(NO_s)$	θ_e(ONO)	r_e(NO (av))	Δr
cc-pVQZ/ROHF	1.2218	110.45	1.4089	1.1344	110.44	1.2717	0.2745
aug-cc-pVQZ/ROHF	1.2216	110.52	1.4087	1.1341	110.50	1.2714	0.2746
cc-pV5Z/ROHF	1.2215	110.49	1.4086	1.1340	110.47	1.2713	0.2746
aug-cc-pV5Z/ROHF	1.2214	110.52	1.4085	1.1339	110.51	1.2712	0.2746
cc-pVQZ/RCISD	1.2424	110.22	1.4341	1.1498	110.02	1.2920	0.2843
aug-cc-pVQZ/RCISD	1.2422	110.27	1.4343	1.1494	110.06	1.2919	0.2849
cc-pV5Z/RCISD	1.2413	110.24	1.4320	1.1489	110.03	1.2905	0.2831
aug-cc-pV5Z/RCISD	1.2412	110.27	1.4320	1.1487	110.06	1.2904	0.2833
cc-pVQZ/UCISD	1.2426	110.22	1.4335	1.1499	110.02	1.2917	0.2836
aug-cc-pVQZ/UCISD	1.2424	110.28	1.4337	1.1496	110.06	1.2917	0.2841
cc-pV5Z/UCISD	1.2415	110.24	1.4314	1.1490	110.03	1.2902	0.2824
aug-cc-pV5Z/UCISD	1.2414	110.27	1.4315	1.1489	110.06	1.2902	0.2826
cc-pVQZ/RCCSD	1.2610	110.01	1.4560	1.1640	109.76	1.3100	0.2920
aug-cc-pVQZ/RCCSD	1.2610	110.07	1.4573	1.1635	109.80	1.3104	0.2938
cc-pV5Z/RCCSD	1.2599	110.03	1.4539	1.1632	109.77	1.3086	0.2907
aug-cc-pV5Z/RCCSD	1.2599	110.06	1.4541	1.1630	109.79	1.3086	0.2911
cc-pVQZ/UCCSD	1.2629	109.99	1.4462	1.1671	109.78	1.3067	0.2791
aug-cc-pVQZ/UCCSD	1.2628	110.05	1.4475	1.1666	109.82	1.3071	0.2809
cc-pV5Z/UCCSD	1.2618	110.00	1.4437	1.1664	109.79	1.3051	0.2773
aug-cc-pV5Z/UCCSD	1.2618	110.04	1.4440	1.1662	109.82	1.3051	0.2778
cc-pVQZ/RCCSD(T)	1.2748	109.88	1.4983	1.1672	109.62	1.3328	0.3311
aug-cc-pVQZ/CCSD(T)	1.2749	109.93	1.5021	1.1664	109.65	1.3343	0.3357
cc-pV5Z/RCCSD(T)	1.2738	109.89	1.4963	1.1664	109.61	1.3314	0.3299
aug-cc-pV5Z/RCCSD(T)	1.2738	109.92	1.4973	1.1662	109.64	1.3318	0.3311
cc-pVQZ/UCCSD(T)	1.2753	109.86	1.4902	1.1695	109.63	1.3299	0.3207
aug-cc-pVQZ/UCCSD(T)	1.2754	109.92	1.4944	1.1685	109.66	1.3315	0.3259
cc-pV5Z/UCCSD(T)	1.2743	109.88	1.4878	1.1688	109.63	1.3283	0.3190
aug-cc-pV5Z/UCCSD(T)	1.2743	109.91	1.4889	1.1685	109.65	1.3287	0.3204
cc-pVQZ/CASSCF	1.2837	110.00	1.5767	1.1603	109.65	1.3685	0.4164
aug-cc-pVQZ/CASSCF	1.2834	110.06	1.5740	1.1602	109.70	1.3671	0.4138
cc-pV5Z/CASSCF	1.2833	110.03	1.5749	1.1600	109.67	1.3675	0.4149
aug-cc-pV5Z/CASSCF	1.2832	110.06	1.5737	1.1601	109.70	1.3669	0.4136
cc-pVTZ/MRCI	1.2805	109.86	1.5042	1.1723	109.63	1.3383	0.3319
aug-cc-pVTZ/MRCI	1.2802	109.92	1.5076	1.1707	109.64	1.3392	0.3369
cc-pVQZ/MRCI	1.2756	109.95	1.4835	1.1713	109.72	1.3274	0.3122
aug-cc-pVQZ/MRCI	1.2755	110.00	1.4838	1.1709	109.75	1.3274	0.3129
DZP/CASSCF, ref 14			1.563	1.185	109.4		
DZP/CCSD, ref 13			1.303	1.274	109.4		
DZP/UHF-CCSD(T), ref 15				1.513	1.183	109.5	
experiment, ref 18	1.339	108.9					

basis set and dynamic correlation effects. The bending frequency reported Shibuya et al.[22] agrees very well with the theoretical bending frequencies, as seen in Table 3. It should be noted that the physical properties determined from the CASSCF wave functions are not quantitatively satisfactory compared to those from the CCSD(T) and ICMRCI methods. In order to predict quantitatively reliable physical properties, the inclusion of dynamic correlation effects are required. The computed antisymmetric stretching frequencies are also in the ballpark of the experimental value of 273 cm^{-1} for the $^2A''$ state.

In Table 4, the isotopic shifts of the three harmonic vibrational frequencies between the $^{14}NO_2$ and $^{15}NO_2$ isotopomers at the CCSD, CCSD(T), and ICMRCI levels of theory as well as the experimental assignments in ref 22 are presented. The magnitude of the isotopic shifts for the three harmonic vibrational modes is in the order $\Delta\omega_1 > \Delta\omega_2 > \Delta\omega_3$. It is seen that the symmetric stretching mode (ω_1) would provide the largest isotopic shift. Among the experimental vibrational energy levels (less than 1746 cm^{-1}), the bands at 970 (1,0,0) and 1690 cm^{-1} (1,1,0) show the largest isotopic shifts. Therefore, it may be possible to make an alternative assignment of the observed frequency of 1690 cm^{-1} [originally assigned as a (1,1,0) band] to be the fundamental band (ν_1) (1,0,0) for the symmetric stretching mode and 970 cm^{-1} [originally assigned as a (1,0,0) band] to be a combination band $\nu_2 + \nu_3$ (0,1,1). However, a detailed vibrational analysis based on the variational method should be carried out in order to make decisive assignments for the observed frequencies.

***C_{2v}* and *C_s* Structures.** The geometrical parameters for the C_{2v} symmetry $\tilde{C}\ ^2A_2$ and C_s symmetry $^2A''$ structures are reported in Table 5. According to the Walsh diagram,[38] the binding energy of the $6a_1$ orbital decreases rapidly with decreasing bond angle. Therefore, the $\tilde{C}\ ^2A_2$ state with two electrons in the $6a_1$ orbital is expected to have a significantly smaller bond angle compared to that of the ground state. At all of the levels of theory, the bond angle of the $\tilde{C}\ ^2A_2$ has indeed been predicted to be smaller, about 110° relative to 134.1° of the $\tilde{X}\ ^2A_1$ ground state.[4,39] The bond length for the $\tilde{C}\ ^2A_2$ stationary point is predicted to be considerably longer than that for the ground state. The elongation of the NO bond distance with correlation effects is mainly due to the excitation from

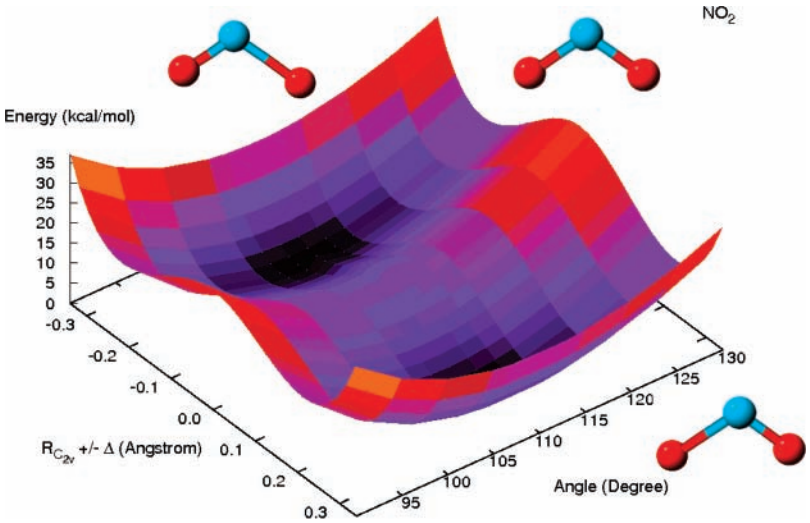

Figure 2. The double minimum nature of the potential energy surface for the $\tilde{C}\ ^2A''$ state of NO_2. The two minima represent the two C_s structures. The transition state represents the C_{2v} structure between the two minima. The energy barrier is 3.6 kcal/mol at the cc-pVTZ/CASSCF level of theory. At the two C_s minima, the two bond distances are $r_e(NO_l) = 1.584$ and $r_e(NO_s) = 1.162$ Å and vice versa, and the equilibrium bond angle is 109.6°.

the NO bonding π orbital ($1b_1$) to the NO antibonding π orbital ($2b_1$), as noted in section II (in Table 1). The bond angle does not differ much between the $^2A_2$ and the $^2A''$ structures. At the aug-cc-pV5Z/UCCSD(T) level of theory, the two NO bond distances for the $\tilde{C}\ ^2A''$ state are predicted to be $r_e(NO_l) = 1.489$ and $r_e(NO_s) = 1.169$ Å, and the ONO band angle is 109.7°. At the best multireference aug-cc-pVQZ/ICMRCI level, the bond distances are $r_e(NO_l) = 1.484$ and $r_e(NO_s) = 1.171$ Å, and the bond angle is 109.8°. The two NO bond distances for the $\tilde{C}\ ^2A''$ state are also elongated with increasing levels of sophistication. The last two columns of Table 5 describe the averaged distance and the difference between the two NO bond distances. These quantities, $r_e(av)$ and Δr, also increase with advanced treatments of correlation effects. The systematic convergence to similar bond distances and angle increases the confidence in the quality of the theoretical structural predictions. The average NO bond distance of 1.329 Å for the $\tilde{C}\ ^2A''$ state [at the aug-cc-pV5Z/UCCSD(T) level of theory] is much closer to the experimental estimate of 1.339 Å from the dispersed fluorescence spectra by Aoki[21] than the NO bond distance of 1.274 Å (with the same method) for the $\tilde{C}\ ^2A_2$ state. The double minimum nature of the potential energy surface of the $\tilde{C}$ state is depicted in Figure 2. The two minima, in Figure 2, represent the two C_s structures, whereas the transition state (saddle point) represents the C_{2v} structure between the two minima. The energy barrier between the C_s and the C_{2v} structures is 3.64 kcal/mol at the cc-pVTZ/CASSCF level of theory. However, at the higher levels of theory, the energy barrier is lowered to 1.53 kcal/mol with the aug-cc-pV5Z/UCCSD(T) method and 1.41 kcal/mol with the aug-cc-pVQZ/ICMRCI method.

Excitation Energies. In Table 6 are reported the excitation energies of the $\tilde{C}\ ^2A_2$ and $\tilde{C}\ ^2A''$ electronic states relative to the $\tilde{X}\ ^2A_1$ ground state. The last column in Table 6 shows the difference between the excitation energies (T_e) of the $\tilde{C}\ ^2A_2$ and $\tilde{C}\ ^2A''$ states. The $\tilde{C}\ ^2A''$ excitation energy increases with more sophisticated treatments of correlation effects. The aug-cc-pV5Z/UCCSD(T) and aug-cc-pVQZ/ICMRCI methods predict the excitation energies (T_e) of the $\tilde{C}\ ^2A''$ state to be 47.5 and 46.7 kcal/mol, respectively, and the difference in excitation energies between the $^2A_2$ and $^2A''$ stationary points is 1.53 and 1.41 kcal/mol, respectively. With the ZPVE corrections, the quantum mechanical excitation energies (T_0 values) for the $\tilde{C}$

TABLE 6: Excitation Energies, T_e (T_0 Values in Parentheses) in kcal/mol of the $\tilde{C}\ ^2A_2$ and $\tilde{C}\ ^2A''$ States Relative to the $\tilde{X}\ ^2A_1$ Ground State of NO_2; ΔE is the Energy Difference between the $\tilde{C}\ ^2A_2$ and $\tilde{C}\ ^2A''$ Stationary Points

level of theory	$\tilde{C}\ ^2A_2$	$\tilde{C}\ ^2A''$	ΔE
cc-pVQZ/ROHF	43.25	25.28(24.31)	17.97
aug-cc-pVQZ/ROHF	43.10	25.09(24.13)	18.01
cc-pV5Z/ROHF	43.20	25.20(24.24)	18.00
aug-cc-pV5Z/ROHF	43.11	25.11(24.15)	18.00
cc-pVQZ/RCISD	48.88	41.60(40.37)	7.28
aug-cc-pVQZ/RCISD	48.68	41.39(40.18)	7.29
cc-pV5Z/RCISD	48.90	41.63(40.42)	7.27
aug-cc-pV5Z/RCISD	48.81	41.54(40.32)	7.27
cc-pVQZ/UCISD	48.67	41.74(40.52)	6.93
aug-cc-pVQZ/UCISD	48.48	41.52(40.31)	6.96
cc-pV5Z/UCISD	48.70	41.76(40.55)	6.94
aug-cc-pV5Z/UCISD	48.61	41.67(40.46)	6.94
cc-pVQZ/RCCSD	47.06	43.03(41.69)	4.03
aug-cc-pVQZ/RCCSD	46.82	42.77(41.44)	4.05
cc-pV5Z/RCCSD	47.04	43.05(41.72)	3.99
aug-cc-pV5Z/RCCSD	46.95	42.95(41.62)	4.00
cc-pVQZ/UCCSD	46.12	43.20(41.81)	2.92
aug-cc-pVQZ/UCCSD	45.90	42.95(41.56)	2.95
cc-pV5Z/UCCSD	46.10	43.22(41.84)	2.88
aug-cc-pV5Z/UCCSD	46.01	43.12(41.73)	2.89
cc-pVQZ/RCCSD(T)	49.42	47.43(46.03)	1.99
aug-cc-pVQZ/RCCSD(T)	49.16	47.13(45.74)	2.03
cc-pV5Z/RCCSD(T)	49.40	47.46(46.06)	1.94
aug-cc-pV5Z/RCCSD(T)	49.29	47.34(45.95)	1.95
cc-pVQZ/UCCSD(T)	49.11	47.54(46.10)	1.57
aug-cc-pVQZ/UCCSD(T)	48.86	47.25(45.81)	1.61
cc-pV5Z/UCCSD(T)	49.09	47.57(46.13)	1.52
aug-cc-pV5Z/UCCSD(T)	48.99	47.46(46.01)	1.53
cc-pVQZ/CASSCF	43.49	39.93(38.59)	3.56
aug-cc-pVQZ/CASSCF	43.24	39.71(38.38)	3.53
cc-pV5Z/CASSCF	43.36	39.82(38.48)	3.54
aug-cc-pV5Z/CASSCF	43.25	39.73(38.40)	3.52
cc-pVTZ/ICMRCI	48.01	46.35(44.90)	1.66
aug-cc-pVTZ/ICMRCI	47.40	45.67(44.24)	1.73
cc-pVQZ/ICMRCI	48.42	47.01(45.53)	1.41
aug-cc-pVQZ/ICMRCI	48.14	46.73(45.25)	1.41
experiment, ref 6	(46.77)	(46.77)	
experiment, ref 21	(46.42)	(46.42)	

$^2A''$ state are determined to be 46.0 kcal/mol (2.00 eV, 16100 cm^{-1}) with the aug-cc-pV5Z/UCCSD(T) method and 45.3 kcal/mol (1.96 eV, 15800 cm^{-1}) with the aug-cc-pVQZ/ICMRCI method, in good agreement with the experimental T_0 values of 46.77 kcal/mol (2.028 eV, 16360 cm^{-1}) by Weaver et al.[6] and 46.42 kcal/mol (2.013 eV, 16234 cm^{-1}) by Aoki et al.[21] In this context, the excitation energies of $T_e = 39.7$ kcal/mol and $T_0 = 38.4$ kcal/mol at the aug-cc-pV5Z/CASSCF level of theory are not quantitatively satisfactory, although the CASSCF wave functions reproduce the quantitatively correct shape of potential energy surface at the C_{2v} stationary point.

V. Concluding Remarks

The Born−Oppenheimer surface of the $\tilde{C}$ state of NO_2 shows double minimum nature with respect to the asymmetric stretching motion and has an asymmetric structure (C_s point group symmetry) with one long and one short NO bond. The C_{2v} symmetry structure is thus actually a transition state between the two asymmetric minima on the potential energy surface of the asymmetric $^2A''$ state. The geometries, harmonic vibrational frequencies, and dipole moments of the $\tilde{C}$ $^2A''$ state are reported in this research at various ab initio levels of theory for future characterization. The excitation energies and bending vibrational frequency evaluated in this research show very good agreement with the experimentally reported values.[6,21,22] Given the sophistication and reliability of the theoretical methods used here, the discrepancy of over 650 cm^{-1} between the experimental fundamental ($\nu_1 = 923$ cm^{-1}) and theoretical harmonic ($\omega_1 = 1641$ cm^{-1}) in-phase stretching frequency of the $\tilde{C}$ $^2A''$ state is a cause of concern, especially considering that the two stretching fundamental frequencies of the NO_2 ground state lie at 1320 and 1618 cm^{-1}. It is possible, however, that the disagreement could be resolved by a reassignment of the observed frequency at 1690 cm^{-1} to the (1,0,0) fundamental and that at 970 cm^{-1} to the combination band (0,1,1), though additional vibronic simulations of the $\tilde{C}$ state spectrum are required to confirm this hypothesis. It is emphasized that inclusion of both static (nondynamic) and dynamic correlation effects and/or high excitations (full triples or more) is requisite in order to investigate the $\tilde{C}$ $^2A''$ state of NO_2 in a qualitatively and quantitatively satisfactory manner.

Acknowledgment. We would like to thank Professor Nicholas C. Handy for his insightful discussions during his spring 2007 visit to the Center for Computational Chemistry. P.P.B. would like to thank Monalisa Bera for help in preparing this manuscript. This research was funded by the Department of Energy, Basic Energy Sciences, Division of Chemical Sciences, Fundamental Interactions Team via Grant DOE FG02-97-ER14748.

References and Notes

(1) Hsu, D. K.; Monts, D. L.; Zare, R. N. *Spectral Atlas of Nitrogen Dioxide*; Academic Press: New York 1978.

(2) Brand, J. C. D.; Chan, W. H.; Hardwick, J. L. *J. Mol. Spectrosc.* **1975**, *56*, 309.

(3) Delon, A.; Jost, R. *J. Chem. Phys.* **1991**, *95*, 5686.

(4) Hardwick, J. L.; Brand, J. C. D. *Chem. Phys. Lett.* **1973**, *21*, 458.

(5) Lafferty, W. J.; Sams, R. L. *J. Mol. Spectrosc.* **1977**, *66*, 478.

(6) Weaver, A.; Metz, R. B.; Bradforth, S. E.; Neumark, D. M. *J. Chem. Phys.* **1989**, *90*, 2070.

(7) Gangi, R. A.; Burnelle, L. *J. Chem. Phys.* **1971**, *55*, 851.

(8) Gillispie, G. D.; Khan, A. U.; Wahl, A. C.; Hosteny, R. P.; Krauss, M. *J. Chem. Phys.* **1975**, *63*, 3425.

(9) Jackels, C. F.; Davidson, E. R. *J. Chem. Phys.* **1976**, *65*, 2941.

(10) Jackels, C. F.; Davidson, E. R. *J. Chem. Phys.* **1976**, *64*, 2908.

(11) Handy, N. C.; Goddard, J. D.; Schaefer, H. F. *J. Chem. Phys.* **1979**, *71*, 426.

(12) Hirsch, G.; Buenker, R. J.; Petrongolo, C. *Mol. Phys.* **1991**, *73*, 1085.

(13) Zimmerman, T.; Koppel, H.; Cederbaum, L. S.; Persch, G.; Demtroder, W. *Phys. Rev. Lett.* **1988**, *61*, 3.

(14) *Multimode Molecular Dynamics Beyond Born−Oppenheimer Approximation*; Koppel, H., Domcke, W., Cederbaum, L. S., Eds.; Wiley and Sons, Inc.: New York, 1984; Vol. 57.

(15) Leitner, D.; Koppel, H.; Cederbaum, L. S. *J. Chem. Phys.* **1996**, *104*, 434.

(16) Kaldor, U. *Chem. Phys. Lett.* **1991**, *185*, 131.

(17) Burton, N. A.; Yamaguchi, Y.; Alberts, I. L.; Schaefer, H. F. *J. Chem. Phys.* **1991**, *95*, 7466.

(18) Crawford, T. D.; Schaefer, H. F. *J. Chem. Phys.* **1993**, *99*, 7926.

(19) Shibuya, K.; Kusumoto, T.; Nagai, H.; Obi, K. *J. Chem. Phys.* **1991**, *95*, 720.

(20) Crawford, T. D.; Stanton, J. F.; Szalay, P. G.; Schaefer, H. F. *J. Chem. Phys.* **1997**, *107*, 2525.

(21) Aoki, K.; Hoshina, K.; Shibuya, K. *J. Chem. Phys.* **1996**, *105*, 2228.

(22) Shibuya, K.; Terauchi, C.; Sugawara, M.; Aoki, K.; Tsuji, K.; Tsuchiya, S. *J. Mol. Struct.* **1997**, *413*, 501.

(23) Crawford, T. D.; Stanton, J. F.; Allen, W. D.; Schaefer, H. F. *J. Chem. Phys.* **1997**, *107*, 10626.

(24) Wiberg, K. B.; Wang, Y.; de Oliveira, A. E.; Perera, S. A.; Vaccaro, P. H. *J. Phys. Chem. A* **2005**, *109*, 466.

(25) Dunning, T. H. *J. Chem. Phys.* **1989**, *90*, 1007.

(26) Kendall, R. A.; Dunning, T. H.; Harrison, R. J. *J. Chem. Phys.* **1992**, *96*, 6796.

(27) Purvis, G. D.; Bartlett, R. J. *J. Chem. Phys.* **1982**, *76*, 1910.

(28) Rittby, M.; Bartlett, R. J. *J. Phys. Chem.* **1988**, *92*, 3033.

(29) Crawford, T. D.; Schaefer, H. F. An Introduction to Coupled Cluster Theory for Computational Chemists. In *Reviews in Computational Chemistry*; Lipkowitz, K. B., Boyd, D. B., Eds.; Wiley-VCH: New York, 2000; Vol. 14; p 33.

(30) Raghabachari, K.; Trucks, G. W.; Pople, J. A.; Head-Gordon, M. *Chem. Phys. Lett.* **1989**, *157*, 479.

(31) Scuseria, G. *Chem. Phys. Lett.* **1991**, *176*, 27.

(32) Werner, H.-J.; Knowles, P. J. *J. Chem. Phys.* **1988**, *89*, 5803.

(33) Werner, H. J.; Knowles, P. J. *MOLPRO*, version 2002.1, a package of ab initio programs; see http://www.molpro.net.

(34) Stanton, J. F.; Gauss, J.; Lauderdale, W. J.; Watts, J. D.; Bartlett, R. J. *ACES2*, Mainz-Austin-Budapest version, a quantum-chemical program package for high level calculations of energies and properties; see http://www.aces2.de.

(35) Crawford, T. D.; Sherrill, C. D.; Valeev, E. F.; Fermann, J. T.; King, R. A.; Leininger, M. L.; Brown, S. T.; Janssen, C. L.; Seidl, E. T.; Kenny, J. P.; Allen, W. D. *J. Comput. Chem.* **2007**, *28*, 1610.

(36) Bera, P. P.; Yamaguchi, Y.; Schaefer, H. F. *J. Chem. Phys.* **2007**, *127*, 174303.

(37) Stanton, J. F. *J. Chem. Phys.* **2001**, *115*, 10382.

(38) Walsh, A. D. *J. Chem. Soc.* **1953**, 2266.

(39) Bowman, W. C.; Lucia, F. C. D. *J. Chem. Phys.* **1982**, *77*, 92.